

## Iron oxide nanoparticles produced by green synthesis supported on the waste crawfish chitosan for dye removal in textile wastewater

Cristina A. De León-Condés<sup>a,\*</sup>, Gabriela Roa-Morales<sup>b</sup>, Gonzalo Martínez-Barrera<sup>c</sup>, Patricia Balderas-Hernández<sup>b</sup>, Bryan Bilyeu<sup>d</sup>

<sup>a</sup>División de Ingeniería Industrial, Tecnológico de Estudios Superiores de Tianguistenco, Carretera Tenango – La Marquesa Km 22, C.P. 52650, Santiago Tianguistenco, Estado de México, México, email: deleoncondes@yahoo.com

<sup>b</sup>Centro Conjunto de Investigación en Química Sustentable, Universidad Autónoma del Estado de México – Universidad Nacional Autónoma de México (UAEM-UNAM), Carretera Toluca-Atlaconulco, km 14.5, Unidad El Rosedal, C.P. 50200, México, emails: gabyroamo@yahoo.com.mx (G. Roa-Morales), patbh2003@yahoo.com.mx (P. Balderas-Hernández)

<sup>c</sup>Laboratorio de Investigación y Desarrollo de Materiales Avanzados (LIDMA), Facultad de Química, Universidad Autónoma del Estado de México, Km 12 de la carretera Toluca-Atlaconulco, San Cayetano 50200, México, email: gonzomartinez02@yahoo.com.mx

<sup>d</sup>Department of Chemistry, Xavier University of Louisiana, 1 Drexel Drive, New Orleans, LA 70125, USA, email: bbilyeu@xula.edu

Received 12 December 2020; Accepted 6 May 2021

### ABSTRACT

Attending to the necessity for developing alternative low-cost processes for removal of wastewater pollutants, in this work iron oxide nanoparticles (FeO-NPs), were supported on chitosan for removal of indigo carmine dye in textile wastewater. The nanoparticles were produced by green synthesis by using extracts of green tea leaves (*Camellia sinensis*), while chitosan was obtained from crawfish shells. Additionally, commercial chitosan was employed (CC). The results show narrow size distribution with 8.17 nm mean diameters for the nanoparticles supported on the commercial chitosan, however when crawfish chitosan was used, the sizes increase up to 73%. Moreover, the adsorption kinetic results were fitted to the pseudo-second-order kinetic model. In the case of the adsorption isotherms, the composites with crawfish chitosan were aligned with the Temkin isotherm, while those with commercial chitosan with the Langmuir isotherm. The addition of the FeO-NPs to commercial chitosan allowed 49.16 mg/g maximum adsorption capacity and 50.2% reduction on the chemical oxygen demand, however, for composites with crawfish chitosan these values decreased, 56% and 33%, respectively. The full removal of indigo carmine dye in textile wastewater occurred at room temperature with 75 mg/L concentration, 7.0 pH, 1 g/L chitosan/FeO-NPs ratio, and 45 min contact time. The chitosan/FeO-NPs composites were characterized by energy-dispersive X-ray spectroscopy, Fourier transforms infrared spectroscopy, scanning electron microscopy, and transmission electron microscopy.

**Keywords:** Chitosan; Iron oxide nanoparticles; Indigo carmine dye; Green synthesis; Textile wastewater

### 1. Introduction

The textile industry consumes large amounts of water for processes involving dyes, which producing high quantities of wastewater. Around 3,600 dyes and 8,000 chemicals

are currently used by the textile industry [1]. Indigo carmine (sodium salt of 5,5'- indigo disulfonic), is one of the most frequent dyes found in the textile industry effluents. It is used in polyester fibers for producing denim articles. However, is recalcitrant and highly toxic to humans. When given intravenously, can cause tumors, severe hypertension, cardiovascular disease, and respiratory problems [2,3].

\* Corresponding author.

Several treatments have been used for the indigo carmine dye degradation, these include: (i) advanced oxidation hydroxyl radical generation (AOP), with which complete mineralization is achieved [4]; (ii) usage of manganese and ferrite nanocomposites with which 98.6% removal is obtained [5]; (iii) Novel fiber membranes with high huge potential for removal [6]; (iv) Combined treatments that include membrane bioreactors, nanofiltration, and reverse osmosis, with which 75% COD is reduced [7]. Such treatments have been successful, however, diminution on the associated operational costs are investigated [8]. Due to this inconvenience, the adsorption process is an effective alternative for the removal of wastewater pollutants; due to its characteristics as being inexpensive, easy to handle, and to provide sludge-free cleaning operations [9,10]. One of the potential materials for such purposes is the crawfish shells, which are natural and inexpensive [11].

The nanoparticles have shown good results in the removal of the dye in textile wastewater, due to the diameter sizes (50–100 nm) and high surface area [12]. Iron oxide nanoparticles (FeO-NPs), have shown significant advantages, as their stability and usage in several environmental problems, for example as oxidizing agents or pollutant adsorbent in wastewater [13]. They are obtained by chemical synthesis, which sometimes produces pollutant compounds, the reason why alternative processes have been used, as synthesis by green chemistry, which is cheap, eco-friendly, and does not require harmful compounds [14].

Furthermore, high improvements on the physicochemical properties are obtained when metal oxide nanoparticles are supported on the surface of another material, as chitosan, porous resins, cellulose, carboxymethyl cellulose, or alginate [15]. Chitosan is an effective adsorbent for the removal of wastewater pollutants [16,17], besides being abundant in nature, low cost, widely available, highly biocompatible, with selective, and chelation capacity as well as being mechanically stable [18].

The aim of this work was to obtain low-cost composites for the removal of indigo carmine dye in textile wastewater. For such purpose, iron oxide nanoparticles were produced by green synthesis, which was supported on chitosan, which was obtained from crawfish shells.

## 2. Experimental

### 2.1. Materials and methods

Crawfish shells were collected from the Mississippi river in New Orleans, USA. They were washed with water for organic matter removal. The dry exoskeletons from the head, legs, and tail were sieved by using 60 mesh (250  $\mu\text{m}$ ).

### 2.2. Reagents

Indigo carmine dye, analytical grade, was purchased from Sigma Aldrich Chemicals; (Sigma Grupo Corporativo Industrial - Calle 6 Norte No. 107 Parque Ind. Toluca 2000, 50200 Toluca de Lerdo, México) while  $(\text{NH}_4)_2\text{Fe}(\text{SO}_4)_2 \cdot 6\text{H}_2\text{O}$ , NaOH, and HCl reagents, analytical grade, were purchased from Sigma Aldrich Alfa Aesar Chemicals. The green tea was from a known trademark, namely Lipton. All solutions were prepared using deionized water.

### 2.3. Extraction of chitosan from crawfish shells

Crawfish shells were grinded until to obtain a fine solid. For the deproteinization and to dissolve fats and proteins attached to the shells, the shells were mixed with NaOH (1M) and stirred at 80°C for 3 h; then they were ground and washed. After, the demineralization was made mixing the shells with 1 M HCl. The obtained chitin was subjected to a deacetylation process with 12.5 M NaOH for 24 h to convert it to chitosan. After, this was washed to obtain neutral pH. Finally, was drying, finely grounding, and sieved with 60 mesh (250  $\mu\text{m}$ ) [19].

### 2.4. Elaboration of the (CC/FeO-NPs) and (CSC/FeO-NPs) composites

In the first stage, 3.25 g  $(\text{NH}_4)_2\text{Fe}(\text{SO}_4)_2 \cdot 6\text{H}_2\text{O}$  was dissolved in 150 mL deionized water along with 5 g chitosan, then such solution was stirred for 3 h. At the same time, the green tea solution (36 g/L) was magnetically stirred at 80°C. Both solutions were mixed and magnetically stirring for 2 h. Finally, the samples were washed with distilled water and dried, as shown in Fig. 1. Two types of chitosan were used, that obtained from crawfish shells (CS) and the chitosan (poly(D-glucosamine)) deacetylated chitin, purchased from Sigma-Aldrich (CC).

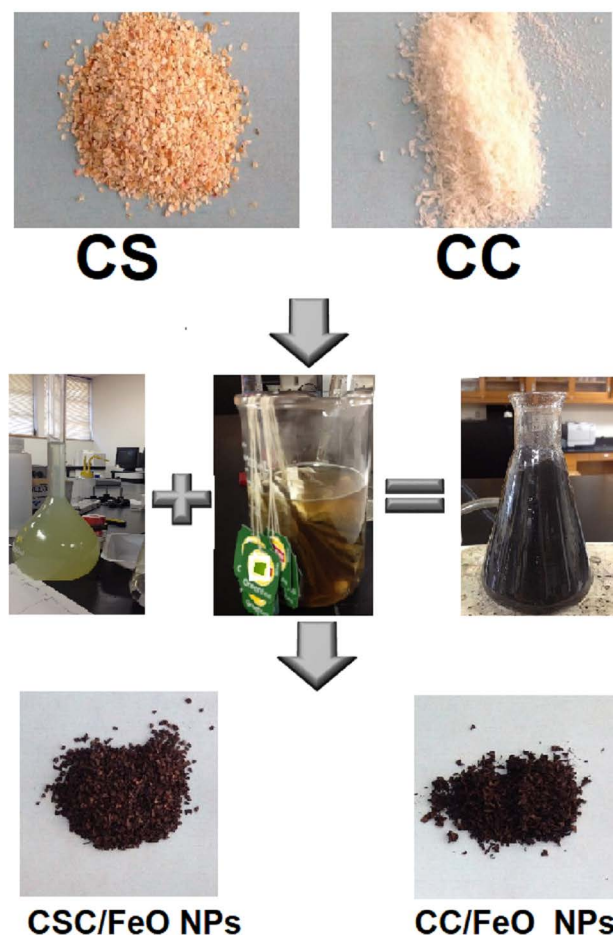


Fig. 1. Elaboration diagram of the composites.

## 2.5. Characterization

Functional groups were analyzed by Fourier transform infrared spectrometry (FT-IR) spectroscopy by Bruker-Tensor 27 equipment with platinum attenuated total reflection accessory (Bruker Mexicana, S.A. de C.V. -Paz Montes de Oca No. 24 Col. General Anaya 03340 Ciudad de México). The surficial morphology was analyzed by scanning electron microscopy (SEM), using a JEOL-5900-LV microscope operated at 20 keV in high-vac mode; coupled to an X-ray energy dispersion probe (EDS) used for the elemental analysis. The size and shape of the FeO nanoparticles were obtained by transmission electron microscopy (TEM), in a JEOL-2100 microscope with a LaB6 filament, operated at 200 keV.

The pH point of zero charge (ZPC) is the pH where the surface charge equals zero ( $\text{pH}_{\text{ZPC}}$ ), it was obtained with a Thermo Scientific Orion Star A325 pH meter (Thermo Scientific – (venta de Thermo Scientific) PRIVADA 10 B SUR #3908 COL. ANZUREZ, C.P. 72530, PUEBLA, PUE), according to the method of Boudouaia [20]. For such purpose, pH of 20 mL 0.01 M NaCl solution is adjusted from 3 to 12 by adding 0.1 M HCl or 0.1 M NaOH solutions. Then, 0.25 g of the chitosan/FeO-NPs composite is added; after such solution is stirring for 24 h, and the pH is measured. The  $\text{pH}_{\text{ZPC}}$  value is obtained graphically from the difference between the final and initial pH [20].

## 2.6. Adsorption kinetics and isotherms

The adsorption kinetic experiments were carried out by mixing 0.05 g chitosan/FeO-NPs with 50 mL indigo carmine dye solution (100 mg/L concentration), at 7.0 pH for 90 min. Samples were collected at different times, covering from 5 to 90 min. For adsorption isotherms experiments, different indigo carmine concentrations were prepared, covering from 10 to 80 mg/L, at room temperature and considering the equilibrium time. Each reaction was repeated three times.

## 2.7. Textile wastewater treatment in the batch system

Textile wastewater samples were collected in glass bottles and placed 4°C. Such samples contain suspended solids,

mineral oils, surfactants, and indigo carmine dye. The samples had 73 mg/L concentration of indigo carmine dye, pH 7.0 (measured with a pH M210 meter), and 2,352 mg/L COD [measured according to the open reflux method, from the American Public Health Association (APHA)]. In 100 mL beakers, mixtures of 50 mL textile wastewater and 0.05 g (chitosan/FeO-NPs) composites were made. Then, they were shaken at 120 rpm and centrifuged. Finally, the dye concentration was measured by UV-vis spectroscopy, using Perkin Elmer Lambda 25 equipment (Perkin Elmer - Macedonio Alcalá No. 54, Guadalupe Inn, C.P. 01020, Ciudad de México).

## 3. Results and discussion

### 3.1. Characterization of the composites

#### 3.1.1. FT-IR spectrometry

FT-IR spectra of chitosan/FeO-NPs composites are shown in Fig. 2. The characteristic bands of chitosan were located at 3,355 and 3,400  $\text{cm}^{-1}$  which corresponding to the N–H bending vibrations of the –OH group; at 2,900  $\text{cm}^{-1}$  (C–H stretching vibration), which is frequently used as a reference band for chitosan [21]; at 1,651 and 1,646  $\text{cm}^{-1}$  (N–H bending vibration), and 1,388  $\text{cm}^{-1}$  (–C–O stretching vibration) of primary alcohol group [22,23]; at 1,073  $\text{cm}^{-1}$  (C–OH stretching vibration), at 1,020  $\text{cm}^{-1}$  (–NH<sub>2</sub> vibration) of the free primary amino group [24]. The Fe–O vibrations were located at 631 and 577  $\text{cm}^{-1}$  [25,26].

#### 3.1.2. SEM analysis

Surfaces of commercial chitosan (CC/FeO-NPs) and crawfish shells chitosan (CSC/FeO-NPs) composites are shown in Fig. 3. In the case of the composites with commercial chitosan (Fig. 3a), spherical particles are agglomerated on the matrix; while for composites with CSC, a rough surface with agglomerated FeO-nanoparticles is observed (Fig. 3b).

Interactions between chitosan and FeO-nanoparticles were confirmed by EDS analysis, due to the Fe and O presence. The atomic mass percentages were 38.4% O, 35.3% C, and 9.2% N (chemical elements of chitosan), and 22.4% Fe,

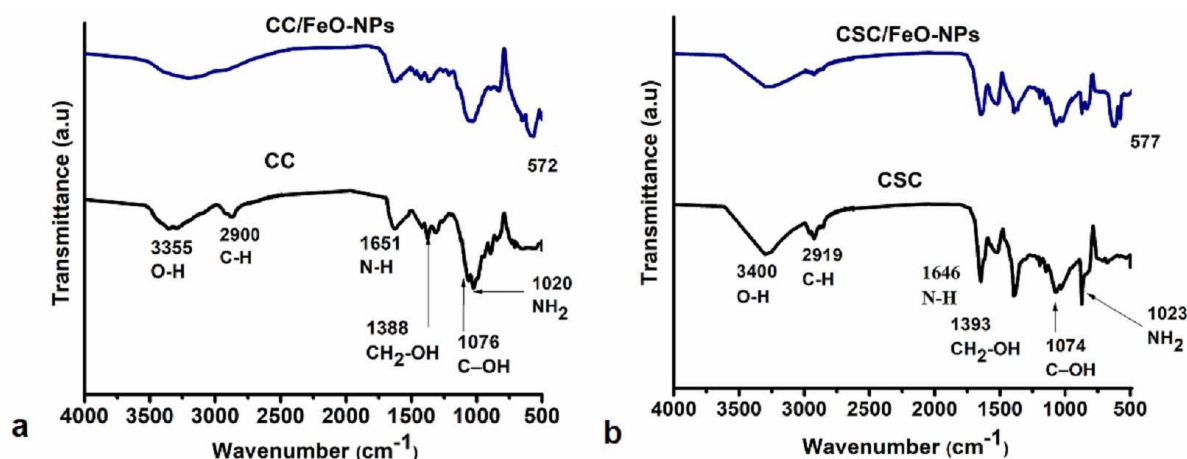


Fig. 2. Fourier transform infrared spectra of (commercial chitosan/FeO-NPs) composite (a), and (crawfish shells chitosan/FeO-NPs) composite (b).

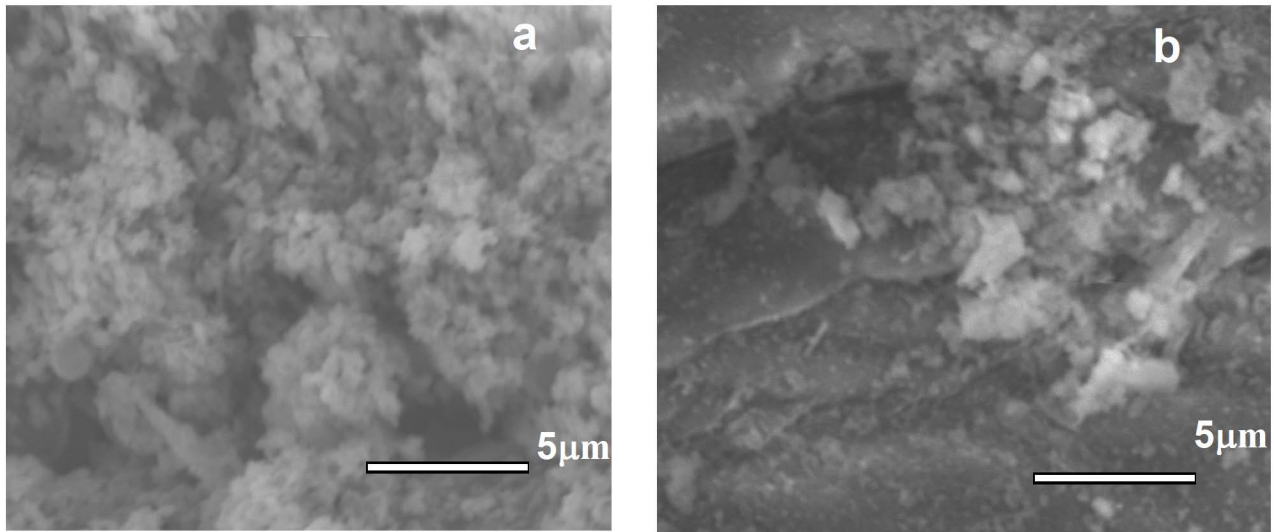


Fig. 3. SEM images of the composites: commercial chitosan/FeO-NPs (a), and crawfish shells chitosan/FeO-NPs (b).

for the composites with commercial chitosan, while for those with crawfish shells, the percentages were lower, namely 33.8% O, 25.3% C, 6.4% N, and 12.2% Fe.

### 3.1.3. Transmission electron microscopy

TEM images of the composites show agglomerated spherical nanoparticles, with 8.17–14.2 nm mean sizes (Fig. 4). Nanoparticles supported on the CSC shown broad size distribution. The mean sizes were 73% bigger than those observed on the commercial chitosan. The bigger nanoparticle sizes for composites with crawfish chitosan were 24 nm, higher than those for commercial chitosan (18 nm). These sizes contributed to the increase in the roughness surface, observed in the SEM images. In reported

studies, similar TEM images were obtained for chitosan/FeO-NPs composites, however, the synthesis method was more expensive compared with ours [27,28].

TEM images demonstrate the presence of the iron oxide nanoparticles, which were promoted by the green tea (*Camellia sinensis*), through its polyphenols which reduce the iron metallic salts, and by the chitosan chelating ability through its positively charged amino group, which can bind or interact with oppositely charged metal ions [26,27].

### 3.2. Adsorption kinetics

The adsorption kinetic results represent the relationship between time and adsorption capacity. The equilibrium time for composites with commercial chitosan was 35 min,

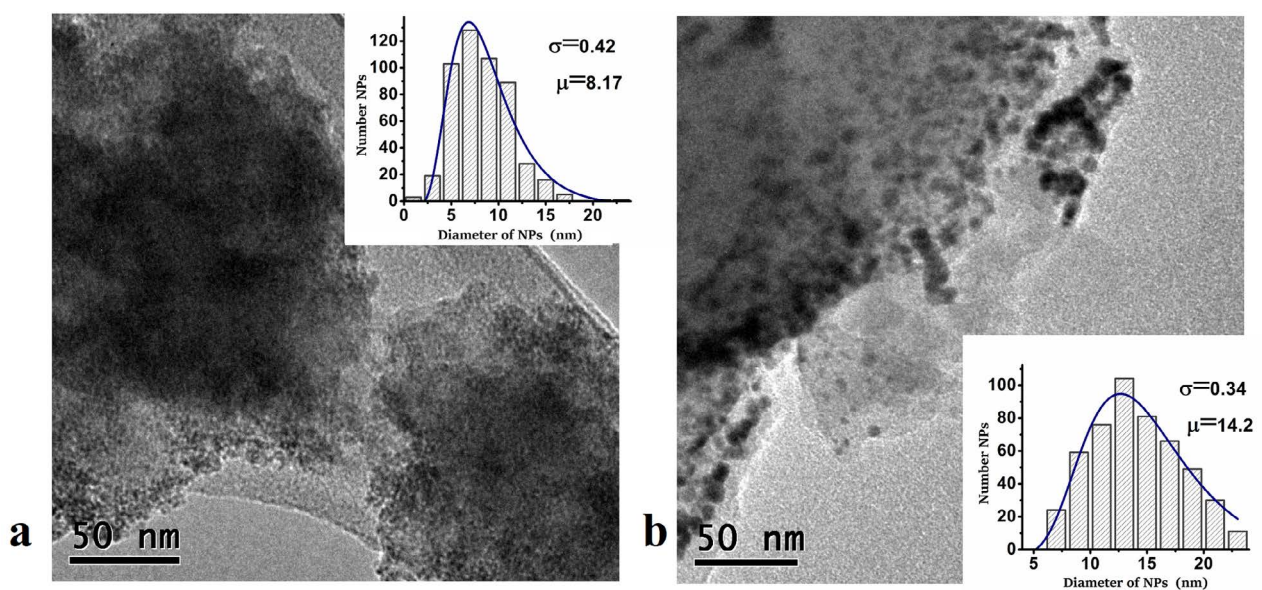


Fig. 4. TEM images of the composites and their particle size distributions: commercial chitosan/FeO-NPs (a), and crawfish shells chitosan/FeO-NPs (b).

while for those with crawfish shells, was 90 min. The adsorption kinetics for the removal of indigo carmine dye were studied in terms of the pseudo-first-order, pseudo-second-order, and second-order kinetics models.

The second-order model fits better with the adsorption kinetics for composites with commercial chitosan, with  $R^2 = 0.998$  correlation coefficient. While for those with crawfish chitosan the better was the pseudo-second-order model, with  $R^2 = 0.990$  correlation coefficient. Such results demonstrate that the adsorption process was carried out through chemical processes. The second-order model parameters for composites with commercial chitosan were  $a = 1.47$  and  $b = 0.52$ , which are lower than those for composites with crawfish chitosan (CSC/FeO-NPs),  $a = 2.83$  and  $b = 0.67$ . Furthermore, the  $q_{exp}$  and  $q_{cal}$  values are very similar,  $q_{exp} = 36.85$  mg/g and  $q_{cal} = 37.07$  mg/g for composites with commercial chitosan, which are higher than those with crawfish shells, namely  $q_{exp} = 28.91$  mg/g and  $q_{cal} = 30.92$  mg/g. Since the values for the “ $a$ ” parameter are higher than those for “ $b$ ”, and that the  $q_{exp}$  and  $q_{cal}$  are very similar, it is concluded that exists a greater tendency to adsorption than desorption.

The  $k_2$  adsorption constant obtained with the pseudo-second-order model,  $k_2 = 0.0473$  was higher for composites with commercial chitosan, than those with crawfish shells,  $k_2 = 0.0453$ , such difference coincides with the employed time for the maximum adsorption capacity. Finally, it important to mention that the same adsorption processes were applied to both types of composites, whereby the adsorption occurrence had the same nature and the adsorption capacity and time were obtained at the equilibrium. Such adsorption processes involving chitosan coincide with those obtained by Gopinathan et al. [29] and Lou et al. [30].

### 3.3. Adsorption isotherm

The indigo carmine adsorption isotherms along with the Langmuir, Freundlich, Langmuir–Freundlich, and Temkin profiles for the composites are shown in Fig. 5, and the isothermal parameters in Table 1. The adsorption capacity of the composites with commercial chitosan (CC/FeO-NPs)

was twice higher than those for composites with crawfish chitosan, which coincides with the adsorption results at the equilibrium, obtained from the adsorption kinetics at initial concentration. The adsorption capabilities were due to the presence of amino and hydroxyl groups.

According to the regression coefficient and the experimental data, the composites with commercial chitosan (CC/FeO-NPs) were better fitting with the Langmuir model. Thus, the adsorption takes place at homogeneous sites on the adsorbent surface [31]. For composites with crawfish chitosan, the better fitting was made with the Temkin model; which confirms that the adsorbate–adsorbent interactions are more significant in the composites with crawfish chitosan than those with commercial chitosan. Even more, composites with crawfish chitosan show higher calculated adsorption heat, but lower coverage degree; which was corroborated by the Langmuir model.

The adsorption was favorable, since the Freundlich parameter ( $1/n$ ) had values between 0 and 1, which is related to the degree of homogeneity, which was higher for composites with commercial chitosan. The  $K_L$  values for composites with commercial chitosan (1.27 mg/L), were higher than those with crawfish chitosan (0.27 mg/L), as well as the adsorption capacity (49.18 mg/g) was higher with respect to those obtained for composites with crawfish (21.25 mg/g).

### 3.4. pH effects and the dye adsorption mechanism

According to some authors, the best removal percentages of indigo carmine dye occurs in an acid medium (pKa 6.4–6.7), since in other mediums these decrease [20,32,33]. Moreover, the better dye adsorption capacity made for chitosan occurs for pH between 4 and 10 [16,34]. In this work, the pH value after the dye adsorption process for both composites was 7.6, which was lower than the calculated  $pH_{ZPC}$  values, 7.8–8.0. Thus, the composites were positively charged and adsorption of anionic indigo carmine occurred easily. That is to say, there exists electrostatic attraction between the negatively charged indigo carmine functional group and the positively charged amine groups on the surface of the chitosan/FeO-NPs composites [20,35].

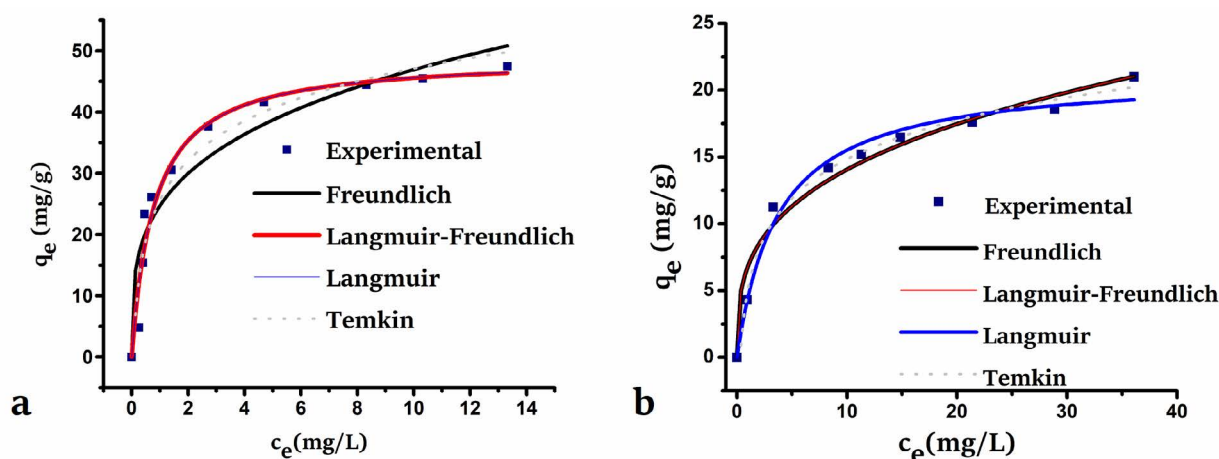


Fig. 5. Adsorption isotherms of the composites: commercial chitosan/FeO-NPs (a), and crawfish shells chitosan/FeO-NPs composites (b) (0–100 mg/L initial dye concentration, 1 g/L adsorbent dosage).

Table 1  
Adsorption isotherm parameters of indigo carmine dye

Adsorption isotherm models	Equation	Parameters	CC/FeO-NPs	CSC/FeO-NPs
Langmuir	$q_e = \frac{q_m K_L C_e}{1 + K_L C_e}$	$q_m$ (mg/g)	49.1827	21.2562
		$K_L$ (L/mg)	1.2703	0.27
		$R^2$	0.9612	0.988
Freundlich	$q_e = K_F C_e^{1/n}$	$K_F$ (mg/g)	24.7164	6.8358
		$1/n$	0.2784	3133
		$R^2$	0.8982	0.9697
Langmuir-Freundlich	$q_e = \frac{K C_e^{1/n}}{1 + a C_e^{1/n}}$	$K$ (mg/g)	46.9415	24.8549
		$a$ (L/mg)	1.5437	0.2739
		$1/n$	0.8424	1.3407
		$R^2$	0.9585	0.9841
Temkin	$q_e = B \ln A_T + B \ln C_e$	$A_T$ (L/mg)	15.4921	3.3884
		$B$ (L/mg)	9.3436	4.2094
		$B$ (J/mol)	265.03	588.30
		$R^2$	0.9462	0.9914

With respect to the adsorption mechanism, several studies have proposed that in an aqueous solution, the first step consist in the acid dye dissolution, since their sulfonate groups ( $\text{DSO}_3\text{Na}$ ) are dissociated and converted to anionic ions, as it is shown in Eq. (1) [33,36–38]:



Moreover, in presence of  $\text{H}^+$ , the  $\text{RNH}_2$  amino group of chitosan are protonated.



Thus, the adsorption process occurs due to the electrostatic attraction produced between the anionic groups of the dyes and the cationic groups of chitosan.



Furthermore, iron oxide nanoparticles contain surficial hydroxyl groups that form hydrogen electrostatic bonds, which enhance the adsorption efficiency [39].

The adsorption process parameters obtained in this work were compared with those reported for composites with chitosan, as it is shown in Table 2.

### 3.5. Dye removal and COD reduction

Full degradation was faster for composites with commercial chitosan (CC/FeO-NPs), employing 40 min compared to the 120 min for composites with crawfish chitosan (Fig. 6a). Such differences are attributed to the chitosan production process by crawfish shells. However, chitosan has a synergistic effect, since acts as an adsorbent and as a supporting material, which favors the catalytic behavior of the iron oxide nanoparticles and the indigo carmine degradation. The dye molecules are adsorbed onto the chitosan and the iron oxide nanoparticles reacted with the textile wastewater, producing electrons that breaking the  $\text{C}=\text{C}$  chromophore bonds in the indigo carmine [43].

The chemical oxygen demand (COD) results confirm the presence of pollutants in textile wastewater. The COD values gradually decrease with time (Fig. 6b). Better efficiency on the reduction values (up to 75.3%), were obtained for composites with commercial chitosan (CC/FeO-NPs), when comparing with those obtained with composites with crawfish chitosan (50.2%).

COD reduction was due to the synergistic effect produced by the adsorption process and the oxidation property of the nanoparticles. Indigo carmine degradation begins with the chromophore cleavage, then with the formation of

Table 2  
Adsorption parameters for iron oxide/chitosan composites

Adsorbent	$q_{e,\text{max}}$ (mg/g)	pH	Contact time (min)	Dye concentration (mg/L)	References
Fly ash-chitosan/graphene oxide	38.8	3	60	Acid Red GR (50 mg/L)	[40]
Chitosan beads	96.15	3	60	Indigo carmine (50 mg/L)	[35]
$\text{Fe}_3\text{O}_4$ -chitosan	20.5	4–6	30	Methyl Orange (20 mg/L)	[41]
$\text{Fe}_3\text{O}_4$ -chitosan	89.7	5.6	120	Reactive Red 141 (134 mg/L)	[42]
FeONPs-commercial chitosan	49.18	7.0	40	Indigo carmine (75 mg/L)	This study
FeONPs-crawfish shells chitosan	21.52	7.0	120	Indigo carmine (75 mg/L)	This study

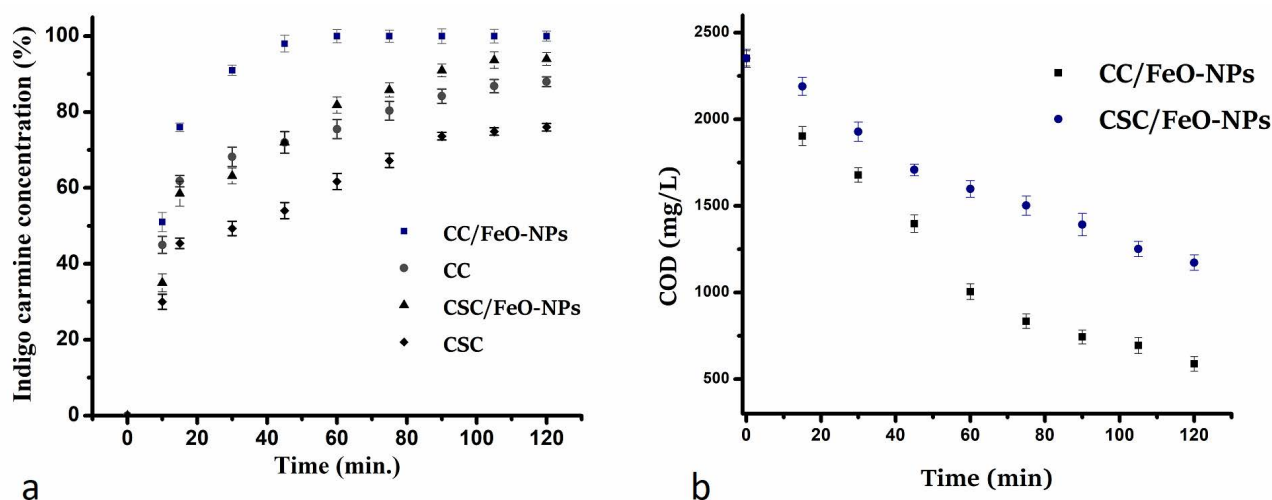


Fig. 6. Indigo carmine dye (a), and COD concentrations (b), of the commercial (chitosan/FeO-NPs) and (crawfish shells chitosan/FeO-NPs) composites (1 g/L adsorbent dose, 100 mL sample volume).

the isatin 5-sulfonic acid (aromatic product). The dye molecules are adsorbed gradually with time on the chitosan surface, but the process becomes slow due to the saturation on the adsorption sites, which is shown by the progressive discoloration of the solution [2,44–46]. The COD reduction values are according to the maximum adsorption capacity obtained, as well as with the homogeneous sites on the adsorbent surface.

#### 4. Conclusions

The effectiveness of this low-cost adsorption process based on the green synthesis for to obtained iron oxide nanoparticles as well as the usage of chitosan obtained from crawfish shells was very favorable, since small nanoparticles (8.17–14.2 nm), maximal adsorption capacities (21.25–49.19 mg/g), and COD reductions (50.2%–75.3%) were obtained. Moreover, the reduction of the indigo carmine dye and the adsorption process for the composites with commercial chitosan was better fitted by the second-order model, while for those with crawfish chitosan was the pseudo-second-order model, which means that the adsorption processes were carried out through chemical processes. There is a need for further research and optimization on the integrated processes, as well as the development of cost-effective adsorbents with a wide range of affinities that can be a potential and efficient alternative for the removal of different types of ions.

#### Acknowledgments

The authors acknowledge the academic support of the Facultad de Química-UAEM, and the CCIQS-(UAEM-UNAM) institutions. One of the authors, De León-Condés, acknowledges the National Council of Science and Technology Mexico (CONACyT) for the Academic Fellowship (called BECA MIXTA) for the research stance at the Xavier University of Louisiana at New Orleans.

#### References

- [1] T. Hussain, A. Wahab, A critical review of the current water conservation practices in textile wet processing, *J. Cleaner Prod.*, 198 (2018) 806–819.
- [2] J. Wang, L. Lu, F. Feng, Improving the indigo carmine decolorization ability of a *Bacillus amyloliquefaciens* laccase by site-directed mutagenesis, *Catalysts*, 7 (2017) 1–10.
- [3] P.C.G. Pereira, R.V. Reimão, T. Pavesi, E.M. Saggiaro, J.C. Moreira, F. Veríssimo Correia, Lethal and sub-lethal evaluation of Indigo Carmine dye and byproducts after TiO<sub>2</sub> photocatalysis in the immune system of *Eisenia andrei* earthworms, *Ecotoxicol. Environ. Saf.*, 143 (2017) 275–282.
- [4] R.O. Ramos, M.V.C. Albuquerque, W.S. Lopes, J.T. Sousa, V.D. Leite, Degradation of indigo carmine by photo-Fenton, Fenton, H<sub>2</sub>O<sub>2</sub>/UV-C and direct UV-C: comparison of pathways, products and kinetics, *J. Water Process Eng.*, 37 (2020) 101535 (1–9), doi: 10.1016/j.jwpe.2020.101535.
- [5] P.A. Ajibade, E.C. Nnadozie, Synthesis and structural studies of manganese ferrite and zinc ferrite nanocomposites and their use as photoadsorbents for indigo carmine and methylene blue dyes, *ACS Omega*, 5 (2020) 32386–32394.
- [6] S.K. Hubadillah, M.H.D. Othman, Z.S. Tai, M.R. Jamalludin, N.K. Yusuf, A. Ahmad, M.A. Rahman, J. Jaafar, S.H.S.A. Kadir, Z. Harun, Novel hydroxyapatite-based bio-ceramic hollow fiber membrane derived from waste cow bone for textile wastewater treatment, *Chem. Eng. J.*, 379 (2020) 122396 (1–12), doi: 10.1016/j.cej.2019.122396.
- [7] N.C. Cinperi, E. Ozturk, N.O. Yigit, M. Kitis, Treatment of woolen textile wastewater using membrane bioreactor, nanofiltration and reverse osmosis for reuse in production processes, *J. Cleaner Prod.*, 223 (2019) 837–848.
- [8] J.A.G. Cardenas, B.E. García, A. Agüera, J.A.S. Pérez, F.M. Agugliaro, Wastewater treatment by advanced oxidation process and their worldwide research trends, *Int. J. Environ. Res. Public Health*, 17 (2020) 170 (1–19), doi: 10.3390/ijerph17010170.
- [9] I. Anastopoulos, I. Pashalidis, Environmental applications of *Luffa cylindrica*-based adsorbents, *J. Mol. Liq.*, 319 (2020) 114127 (1–9), doi: 10.1016/j.molliq.2020.114127.
- [10] C. Arora, S. Soni, S. Sahu, J. Mittal, P. Kumar, P.K. Bajpai, Iron based metal organic framework for efficient removal of methylene blue dye from industrial waste, *J. Mol. Liq.*, 284 (2019) 343–352.
- [11] S. Dawood, T.K. Sen, Review on dye removal from its aqueous solution into alternative cost effective and non-conventional adsorbents, *J. Chem. Process Eng.*, 1 (2014) 104 (1–11).

- [12] A. Hamdy, M.K. Mostafa, M. Nasr, Zero-valent iron nanoparticles for methylene blue removal from aqueous solutions and textile wastewater treatment, with cost estimation, *Water Sci. Technol.*, 78 (2018) 367–378.
- [13] P. Xu, G.M. Zeng, D.L. Huang, C.L. Feng, S. Hu, M.H. Zhao, C. Lai, Z. Wei, C. Huang, G.X. Xie, Z.F. Liu, Use of iron oxide nanomaterials in wastewater treatment: a review, *Sci. Total Environ.*, 424 (2012) 1–10.
- [14] H.M. Fahmy, F.M. Mohamed, M.H. Marzouq, A.B.E.D. Mustafa, A.M. Alsoudi, O.A. Ali, M.A. Mohamed, F.A. Mahmoud, Review of green methods of iron nanoparticles synthesis and applications, *Bionanoscience*, 8 (2018) 491–503.
- [15] A.B. Flores, H.P.T. Jaldin, A.R.V. Néstor, G.L. Téllez, V.S. Mendieta, D.M.Á. Márquez, Metallurgical slag properties as a support material for bimetallic nanoparticles and their use in the removal of malachite green dye, *Adv. Powder Technol.*, 31 (2020) 2853–2565.
- [16] B. Tanhaei, A. Ayati, M. Lahtinen, M. Sillanpää, Preparation and characterization of a novel chitosan/Al<sub>2</sub>O<sub>3</sub>/magnetite nanoparticles composite adsorbent for kinetic, thermodynamic and isotherm studies of Methyl Orange adsorption, *Chem. Eng. J.*, 259 (2015) 1–10.
- [17] J. Wang, S. Zhuang, Removal of various pollutants from water and wastewater by modified chitosan adsorbents, *Crit. Rev. Environ. Sci. Technol.*, 47 (2017) 2331–2386.
- [18] M.M. Khin, A.S. Nair, V.J. Babu, R. Murugan, S. Ramakrishna, A review on nanomaterials for environmental remediation, *Energy Environ. Sci.*, 5 (2012) 8075–8109.
- [19] R.S.C.M.D.Q. Antonino, B.R.P.L. Fook, V.A.D.O. Lima, R.I.D.F. Rached, E.P.N. Lima, R.J.D.S. Lima, C.A.P. Covas, M.V.L. Fook, Preparation and characterization of chitosan obtained from shells of shrimp (*Litopenaeus vannamei* Boone), *Mar. Drugs*, 15 (2017) 1–12.
- [20] N. Boudouaia, Z. Bengharez, S. Jellali, Preparation and characterization of chitosan extracted from shrimp shells waste and chitosan film: application for Eriochrome black T removal from aqueous solutions, *Appl. Water Sci.*, 9 (2019) 1–12.
- [21] N.R. Pires, P.L.R. Cunha, J.S. Maclel, A.L. Angelim, V.M.M. Melo, R.C.M. De Paula, J.P.A. Feitosa, Sulfated chitosan as tear substitute with no antimicrobial activity, *Carbohydr. Polym.*, 91 (2013) 92–99.
- [22] A. Kavitha, H.G. Prabu, S.A. Babu, Synthesis of low-cost iron oxide: chitosan nanocomposite for antibacterial activity, *Int. J. Polym. Mater. Polym. Biomater.*, 62 (2013) 45–49.
- [23] L. Tingyi, Z. Wang, L. Zhao, X. Yang, Enhanced chitosan/Fe<sup>0</sup> – nanoparticles beads for hexavalent chromium removal from wastewater, *Chem. Eng. J.*, 189 (2012) 196–202.
- [24] M. Prabakaran, R. Jayakumar, Chitosan-graft-β-cyclodextrin scaffolds with controlled drug release capability for tissue engineering applications, *Int. J. Biol. Macromol.*, 44 (2009) 320–325.
- [25] S.W. Hwang, A. Umar, G.N. Dar, S.H. Kim, R.I. Badran, Synthesis and characterization of iron oxide nanoparticles for phenyl hydrazine sensor applications, *Sens. Lett.*, 12 (2014) 97–101.
- [26] Y. Wen, J. Ma, J. Chen, C. Shen, H. Li, W. Liu, Carbonaceous sulfur-containing chitosan-Fe(III): a novel adsorbent for efficient removal of copper(II) from water, *Chem. Eng. J.*, 259 (2015) 372–380.
- [27] A. Diaz-Hernández, J. Gracida, B.E.G. Almendárez, C. Regalado, R. Núñez, A.A. Reyes, Characterization of magnetic nanoparticles coated with chitosan: a potential approach for enzyme immobilization, *J. Nanomater.*, 2018 (2018) 1–11.
- [28] A. Vaanamudan, M. Sarkar, M. Sadhu, P.S. Pamidimukkala, Clusters of superparamagnetic iron oxide nanoparticles capped with palm shell extract and modified with chitosan: catalytic applications for degradation of cationic and anionic dyes and their binary mixtures, *J. Environ. Chem. Eng.*, 7 (2019) 103244 (3–35), doi: 10.1016/j.jece.2019.103244.
- [29] R. Gopinathan, A. Bhowal, C. Garlapati, Adsorption studies of some anionic dyes adsorbed by chitosan and new four-parameter adsorption isotherm model, *J. Chem. Eng. Data*, 64 (2019) 2320–2328.
- [30] T. Lou, X. Yan, X. Wang, Chitosan coated polyacrylonitrile nanofibrous mat for dye adsorption, *Int. J. Biol. Macromol.*, 135 (2019) 919–925.
- [31] L. Zhai, Z. Bai, Y. Zhu, B. Wang, W. Luo, Fabrication of chitosan microspheres for efficient adsorption of methyl orange, *Chin. J. Chem. Eng.*, 26 (2018) 657–666.
- [32] Z. Harrache, M. Abbas, T. Aksil, M. Trari, Thermodynamic and kinetics studies on adsorption of Indigo Carmine from aqueous solution by activated carbon, *Microchem. J.*, 144 (2019) 180–189.
- [33] D.H.K. Reddy, S.M. Lee, Application of magnetic chitosan composites for the removal of toxic metal and dyes from aqueous solutions, *Adv. Colloid Interface Sci.*, 201–202 (2013) 68–93.
- [34] C.C. dos Santos, R. Mouta, M.C.C. Junior, S.A.A. Santana, H.A. dos Santos Silva, C.W.B. Bezerra, Chitosan-edible oil based materials as upgraded adsorbents for textile dyes, *Carbohydr. Polym.*, 180 (2018) 182–191.
- [35] J.K. Fatombi, E.A. Idohou, S.A. Osseni, I. Agani, D. Neumeyer, M. Verelst, R. Mauricot, T. Aminou, Adsorption of Indigo carmine from aqueous solution by chitosan and chitosan/activated carbon composite: kinetics, isotherms and thermodynamics studies, *Fibers Polym.*, 20 (2019) 1820–1832.
- [36] Y.C. Wong, Y.S. Szeto, W.H. Cheung, G. McKay, Adsorption of acid dyes on chitosan – equilibrium isotherm analyses, *Process Biochem.*, 39 (2004) 695–704.
- [37] A. Shajahan, S. Shankar, A. Sathiyaseelan, K.S. Narayan, V. Narayanan, V. Kaviyaranan, S. Ignacimuthu, Comparative studies of chitosan and its nanoparticles for the adsorption efficiency of various dyes, *Int. J. Biol. Macromol.*, 104 (2017) 1449–1458.
- [38] W.H. Cheung, Y.S. Szeto, G. McKay, Enhancing the adsorption capacities of acid dyes by chitosan nano particles, *Bioresour. Technol.*, 100 (2009) 1143–1148.
- [39] T.K. Saha, N.C. Bhoumik, S. Karmaker, M.G. Ahmed, H. Ichikawa, Y. Fukumori, Adsorption of methyl orange onto chitosan from aqueous solution, *J. Water Resour. Prot.*, 02 (2010) 898–906.
- [40] G. Sheng, S. Zhu, S. Wang, Z. Wang, Removal of dyes by a novel fly ash-chitosan-graphene oxide composite adsorbent, *RSC Adv.*, 6 (2016) 17987–17994.
- [41] F. Hosseini, S. Sadighian, H.H. Monfared, N.M. Mahmoodi, Dye removal and kinetics of adsorption by magnetic chitosan nanoparticles, *Desal. Water Treat.*, 57 (2016) 24378–24386.
- [42] J. Jaafari, H. Barzanouni, S. Mazloomi, N.A.A. Farahani, K. Sharafi, P. Soleimani, G.A. Haghghat, Effective adsorptive removal of reactive dyes by magnetic chitosan nanoparticles: kinetic, isothermal studies and response surface methodology, *Int. J. Biol. Macromol.*, 164 (2020) 344–355.
- [43] Z. Zhao, L. Wang, J. Fan, Y. Song, G. Chu, L. Shao, Degradation of indigo carmine by coupling Fe(II)-activated sodium persulfate and ozone in a rotor-stator reactor, *Chem. Eng. Process. Process Intensif.*, 148 (2020) 107791 (1–6), doi: 10.1016/j.cep.2019.107791.
- [44] S. Ammar, R. Abdelhedi, C. Flox, C. Arias, E. Brillas, Electrochemical degradation of the dye indigo carmine at boron-doped diamond anode for wastewaters remediation, *Environ. Chem. Lett.*, 4 (2006) 229–233.
- [45] K.P.V. Lekshmi, S. Yesodharan, E.P. Yesodharan, MnO<sub>2</sub> efficiently removes indigo carmine dyes from polluted water, *Heliyon*, 4 (2018) e00897 (1–52), doi: 10.1016/j.heliyon.2018.e00897.
- [46] A.B. Flores, A.C. Cruz, E.G. Segura, V.S. Mendieta, D.A.S. Casados, M.A.G. Guirado, R.B. González, Efficient removal of crystal violet dye from aqueous solutions by vitreous tuff mineral, *Environ. Technol.*, 35 (2014) 1508–1519.